npj | flexible electronics

Article

Published in partnership with Nanjing Tech University

https://doi.org/10.1038/s41528-024-00307-1

# Stroke-volume-allocation model enabling wearable sensors for vascular age and cardiovascular disease assessment



Shirong Qiu [1], Bryan P. Y. Yan[2] & Ni Zhao [1]

Frequent and unobtrusive monitoring of cardiovascular conditions with consumer electronics is a widely pursued goal, since it provides the most economic and effective way of preventing and managing cardiovascular diseases (CVDs) — the leading causes of death worldwide. However, most current wearable and flexible devices can only support the measurement of one or two types of vital signs, such as heart rate and blood oxygen level, due to the lack of physiological models to link the measured signals to cardiovascular conditions. Here, we report a stroke-volume allocation (SVA) model to quantify the cushioning function of arteries and empower nearly all existing cardiac sensors with new functions, including arterial stiffness evaluation, dynamic blood pressure tracking and classification of CVD-related heart damage. Large-scale clinical data testing involving a hybrid dataset taken from 6 hospitals/research institutes (9 open databases and 4 self-built databases from 878 subjects in total) and diverse measurement approaches was carried out to validate the SVA model. The results show that the SVA-based parameters correlate well with the gold-standard measurements in arterial stiffness and blood pressure and outperform the commonly used vital sign (e.g., blood pressure) alone in detecting abnormalities in cardiovascular systems.

Population ageing and prevalence of cardiovascular diseases (CVD) have imposed enormous economic and societal burden worldwide[1–3]. Low-cost and mobile health-monitoring devices that can be deployed to individuals for early detection or longitudinal monitoring of CVDs will allow for timely intervention and treatment. Wearable devices that are currently commercially available or that have been developed in laboratories use various techniques for the monitoring of basic vital signs, including electrocardiogram (ECG)[4] for heart rate monitoring and atrial fibrillation detection, epidermal pulse[5] for heart rate and pressure measurement, and photoplethysmography (PPG)[6,7] for heart rate and blood oxygen level monitoring (Fig. 1a). Although these vital signs are essential physiological parameters, they are still inadequate for a comprehensive evaluation of potential CVDs due to the lack of readily available indicators for the vascular dysfunction often linked with such conditions[8–10]. Furthermore, most wearable and flexible sensors only capture a single physiological parameter due to the limitation of the physiological models used.

In this work, we introduce a stroke-volume allocation (SVA) model that enables the application of wearable and flexible sensors for simultaneous evaluation of arterial stiffness (AS), dynamically tracking blood pressure and assessing CVD-related heart damage (CHD). AS reflects generalized thickening and stiffening of arterial walls, which results in the gradual loss of arterial compliance or the cushioning function of healthy elastic arteries[9]. Ageing-induced reduction of arterial wall elastic component is a major cause of high AS, which is associated with increased risk of CVD[11]. However, the conventional method of AS measurement, i.e., the carotid–femoral pulse wave velocity (cfPWV) test, cannot be performed by wearable and flexible devices; the test must be performed by a medical professional on a patient lying supine in a quiet environment[12].

Conversely, the SVA measurement method proposed herein is simple. Specifically, the SVA-based AS (SVA-AS) assessment requires only passive measurements made by a single wearable device for continuous cardiac rhythm monitoring and a once-daily blood pressure (BP) measurement. Hence, the method could be used with various cardiac sensors (Fig. 1a). Changes in BP are a key factor predicting CVD events, especially in individuals with hypertension and poor cardiovascular function[10]. Although the well-known pulse transit time (PTT) and data-driven BP measurement methods can achieve continuous cuffless monitoring, whether these wearable devices have sufficient performance to replace intermittent cuff-based

[1]The Department of Electronic Engineering, The Chinese University of Hong Kong, Hong Kong SAR, China. [2]The Division of Cardiology, Department of Medicine and Therapeutics, The Chinese University of Hong Kong, Hong Kong SAR, China. e-mail: nzhao@ee.cuhk.edu.hk

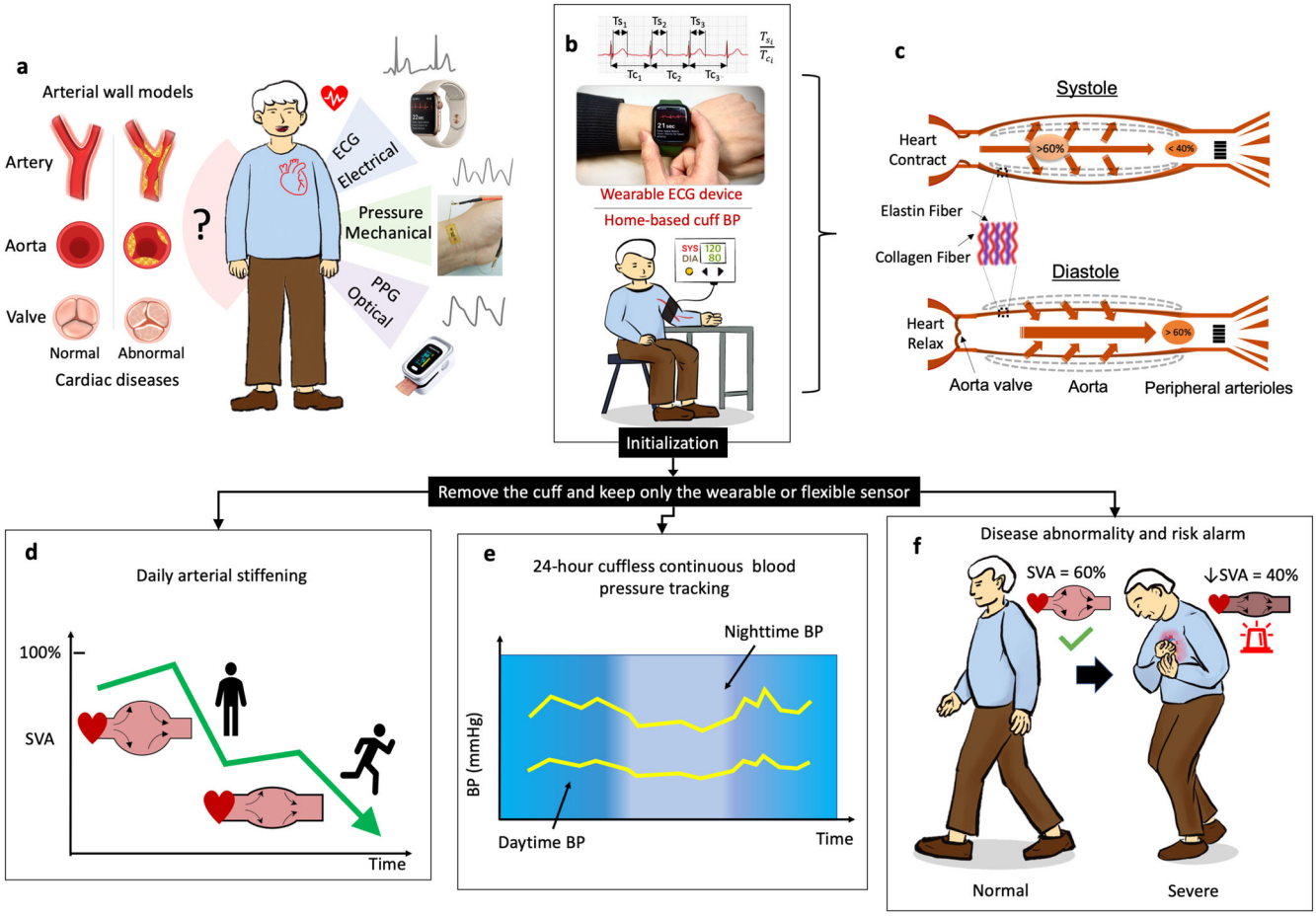


**Fig. 1 | Overview of stroke-volume allocation (SVA) measurement system for arterial wall risk assessment. a** Arterial wall models for health and diseased cardiovascular systems and examples of wearable and flexible cardiac sensors. Reprinted with permission from ref. 5 Copyright 2017 Wiley. **b** Illustration of a daily SVA measurement performed using a wearable ECG device and a home cuff-based BP monitor. **c** Physiological model of stroke volume distribution within one heartbeat cycle (i.e., within systole and diastole phases). **d–f** Illustration on SVA model enabled (**d**) daily arterial stiffening evaluation, (**e**) 24-h BP tracking, and (**f**) alarming of CVD-related heart damage.

measurements is still being debated[13,14]. One of the main problems with these methods is that they cannot precisely interpret BP-related hemodynamics from the crosstalk between macrocirculation and microcirculation, which may result in their performance decreasing over time[14]. By contrast, the proposed SVA model directly describes the dynamic changes in blood volume distribution between the elastic arteries and peripheral arterioles during each heartbeat cycle (Fig. 1c), and this description facilitates the tracking of changes in BP.

A framework of risk of arterial wall dysfunction for using wearable devices to assess SVA-based AS, BP, and CHD abnormalities is presented in Fig. 1. In practice, SVA measurements are performed by a wearable device (e.g., by recording an ECG with an Apple Watch) and a cuff-based BP measurement device, as shown in Fig. 1b. By combining a single BP measurement with continuous cardiac monitoring, an SVA-AS measurement can be made for various daily activities (Fig. 1d). Furthermore, by accumulating measurement points, a transformation between the SVA and the pulse stiffening of blood pressures can be constructed to obtain a reliable SVA-BP model for 24-h BP tracking (Fig. 1e). Finally, by statistically distinguishing the elasticity of the arterial walls of subjects with and without CHD through the SVA measurements, a CHD assessment model can be established for disease alert (Fig. 1f).

In order to realize the application scenarios in Fig. 1, we conducted both theoretical and clinical studies to validate the SVA model and enable its use with wearable platforms with both rigid and flexible sensing units. First, the physiological model for SVA extraction was established and the correlations of SVA with clinically determined cfPWV, BP and CHD were validated. Next, we revealed that the cardiac parameters in the SVA model can be obtained with a variety of sensors, namely flexible epidermal pressure, PPG, and ECG sensors. Based on the discoveries, we demonstrated that the SVA model can readily extend the functions of current commercial wearable devices (such as smart watches), enabling assessment of dynamic arterial stiffening and vascular aging, continuous tracking of BP and identification of CHD. The SVA-based tools for alerting patients to high arterial wall risk can be used to increase early access to CVD surveillance worldwide.

## Results

### Relation between SVA and arterial wall stiffening

Figure 2a presents the mechanisms underlying the correlations between SVA (i.e., the cushioning function of arteries) and ageing-induced arterial wall stiffening, SVA and BP as well as SVA and CHD severity[9]. Vascular tissue mainly comprises elastin, vascular smooth muscle, and collagen; hence, the total Young's modulus of an artery is the combined elastic strength of these components[15]. In general, elastin and collagen contribute to the static arterial Young's modulus, whereas vascular smooth muscle dynamically adjusts the degree of AS under transient neural or hormonal influences[16]. An experimental study revealed that the Young's modulus of elastin fibers $E_e$ is much smaller than that of collagen fibers $E_c$ (i.e., $E_e \sim 1/1000\ E_c$)[17]. Hence, the Young's modulus $E$ of an artery can be expressed as the composition of the recruitment fraction of elastic and collagen fibers and a constant contribution from vascular smooth muscle (denoted $\zeta$) under a

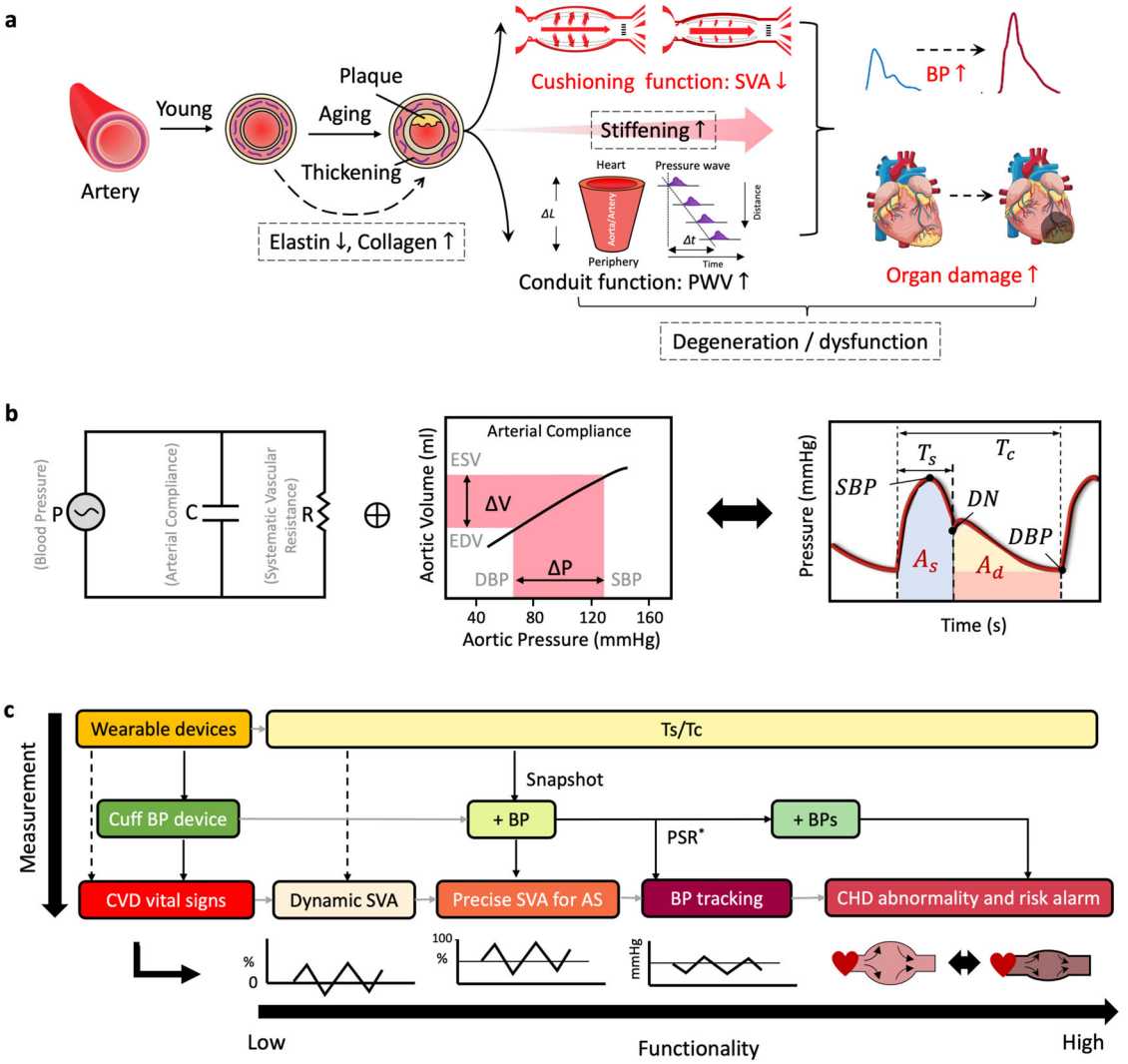


**Fig. 2 | Working principles and modeling and measurement procedure of SVA. a** The correlation of the cushioning and conduit functions with ageing-induced arterial wall stiffening, BP variation and organ damage. **b** SVA extraction model. **c** SVA measurement process for wearable devices.

holding internal pressure in the artery as follows:

$$E = E_c \cdot x_c + E_e \cdot x_e + \zeta \quad (1)$$

where $x_c$ and $x_e$ are the volume fractions of elastin and collagen fibers, respectively, and $x_c = 1 - x_e$. The proportion of elastic fibers in a large artery decreases with age[18]; accordingly, the aorta becomes stiffer. Vascular mechanics analysis (Supplementary Note 1) indicates that when the aorta is stiff, vessels are dilated to a smaller radius compared with the radius of an elastic aorta under the same pressure conditions; this results in a lower buffer volume stored in the aorta. Thus, the essential difference in AS between an elastic and stiff aorta generally leads to a change in the cushioning function of elastic arteries. Notably, an increase in AS accelerates BP elevation and is associated with adverse clinical outcomes, such as CVDs associated with myocardial infarction (MI)[19] and valvular aortic stenosis (VAS)[20].

## SVA Model

For quantifying the cushioning function of an artery, we propose a basic SVA model (Fig. 2b), which is an extension of the Windkessel model of the cardiovascular system[21]. The classical two-element Windkessel model is constructed from the total arterial compliance and peripheral resistance; the arterial compliance mainly buffers the blood volume then support adequate energy to organ during the diastolic phase, whereas the resistance is the peripheral vascular resistance (Fig. 2b left). In contrast to the conduit function of pulse propagation along the arterial tree in the cfPWV method, the cushioning function of elastic arteries buffers the energy released from the heart and supports the provision of blood volume to target organs within a heartbeat cycle. Hence, the SVA, or the blood volume distribution in the circulation, can be defined as the ratio of the stroke volume in the arterial compliance during the systole phase to the total stroke volume pumped by the heart during the same cardiac cycle[22]. Mathematically, SVA is derived from the static aortic compliance (i.e., $C = SV/PP$, where $C$ is the arterial compliance, $SV$ is the stroke volume, and $PP$ is the pulse pressure[23]; Fig. 2b middle) in the constrained Windkessel model (detailed derivation in Supplementary Note 2). Hence, the SVA equals the area ratio of the BP waveform (Fig. 2b right, Methods and Supplementary Note 3).

$$SVA = \frac{SV_c}{SV} = \frac{A_d}{A_s + A_d} \quad (2)$$

where $SV_c$ is the stored volume of the aorta during the systolic period, $SV$ is the stroke volume during each heartbeat, and $A_d$ and $A_s$ are the areas of the BP waveform during the diastolic and systolic phases, respectively.

In practice, to calculate the SVA, we further modeled the ratio of the BP waveform area from Eq. (2) as a function of the systolic duration $T_s$ and

cardiac duration $T_c$ (Supplementary Note 4) as follows:

$$SVA \triangleq \delta \cdot \left(1 - \frac{T_s}{T_c}\right) \tag{3}$$

where $\delta = \frac{DBP}{MBP} \cdot \kappa$. Here the constant factor $\kappa$ is the ratio of the area under the diastolic BP curve to the rectangularized pressure area during the diastolic period (pink region in Fig. 2b right) and can be computed from a single BP measurement; $MBP$ is the mean BP; $\delta$ is a constant that varies between individuals and is related to BP values (e.g., Supplementary Equation (23)); and $T_s/T_c$ is the primary variable that affects the SVA.

Furthermore, because of the lower percentage of the elastic component in the peripheral muscular conduit arteries than the central elastic arteries[24], the central arteries are expected to have a superior cushioning function than the peripheral muscular conduit arteries (Supplementary Note 5); hence, $SVA_{central} > SVA_{peripheral}$.

Finally, by introducing the pulse stiffening relationships between the systolic BP (SBP), dicrotic notch pressure, and diastolic BP (DBP) in the basic SVA model, we can link the SVA with BP (Supplementary Note 6) as follows:

$$BP = \frac{b_s^* - SVA \cdot b}{SVA(PSR - 1) + 1 - k_s^*} \tag{4}$$

where $b_s^*$ and $k_s^*$ are linear coefficients relating DBP and dicrotic notch pressure $P_s^{dn}$, whereas $PSR$ (i.e., pulse stiffening ratio) and $b$ are linear coefficients relating DBP and SBP[25]. All of these coefficients (i.e., $b_s^*$, $b$, $PSR$ and $k_s^*$) are stable for more than 24 h because systolic, diastolic and dicrotic notch BP are influenced by similar factors, such as physical activity, respiratory rhythm, and stress, and thus fluctuate simultaneously[26]. More details regarding the SVA-BP model and $PSR$ are available in Supplementary Notes 6 and 9. In addition, because both the SVA and cfPWV change with BP, an inverse relationship between the SVA and cfPWV can be constructed (Supplementary Note 7).

### Clinical validation of SVA model and SVA-based AS, BP and CHD assessment

Based on the physiological model illustrated in Fig. 2a, we propose two hypotheses that lay the theoretical foundation of our SVA based measurements: 1) SVA is lower in the distal artery than in the central artery and 2) SVA (i.e., the area ratio of the BP curve) can be modeled using Eq. (3), which is primarily related to $T_s/T_c$. Proving the first hypothesis requires verification that SVA decreases along the arterial tree because of the lower elastic component in the peripheral arteries[24]. Proving the second hypothesis requires verification that SVA is related to $T_s/T_c$ measurements. Accordingly, invasive central aortic and peripheral radial continuous BP measurements of patients were performed at the Prince of Wales Hospital, Hong Kong. The measurement sites and BP waveforms are shown in Fig. 3a and b. The SVA is calculated using the area ratio of the BP waveform, as described in Eq. (2). The result shows a higher SVA in the aortic artery (orange circle) than in the radial artery (blue circle) (Fig. 3c), which is consistent with our first hypothesis. Furthermore, using Eq. (3), the SVA in both the aorta (red star) and radial artery (purple star) can be precisely predicted from $T_s/T_c$ with a linear regression. We further analyzed these two parameters in an open MIMIC-I data set, which includes an average of more than 20 h continuous recording of physiological vital signs and BP waveforms for nine ICU patients. Similar case-by-case relationships between SVA and $T_s/T_c$ are found (Supplementary Fig. 1), and a linear relationship between the dynamic range of $T_s/T_c$ [i.e., $\max(T_s/T_c) - \min(T_s/T_c)$] and the dynamic range of SVA [i.e., $\max(SVA) - \min(SVA)$] is identified (Fig. 3d; $r = 0.9705$, $p = 1.41 \times 10^{-5}$).

Subsequently, we conducted SVA-AS and SVA-CHD risk correlation studies on mixed open clinical datasets; the measured parameters are listed in Supplementary Table 1 under IDs 6–13. The snapshot SBP and DBP (measured from an auscultatory or oscillometric device) were used to calculate the person-specific constant $\delta$ in Eq. (3); thus enabling the calculation of SVA by combining the constant with dynamic $T_s/T_c$. Once SVA is determined, the AS can be immediately evaluated, and as will be illustrated later, the combination of SVA with its related hemodynamic parameters can be used to well predict the static CVD risk. Figure 3e unambiguously reveals the inverse relationship between cfPWV and SVA; the regression line is expressed as $\text{cfPWV} = -0.396 \times \text{SVA} + 33.195$ ($r = -0.7899$, $p = 9.63 \times 10^{-5}$) and the precise expression is $\text{cfPWV} = \sqrt{\left[\frac{1.048 + 1.188 \cdot SVA}{SVA(1.03592 - 1) + 1 - 1.01666} + 0.4079\right]/0.9965}$ (see detailed description in Supplementary note 7). This inverse relation connects the cushioning and conduit functions, which represent the two basic properties of arteries, e.g., an increased PWV and a decreased SVA both point to vascular ageing. We next compared SVA in healthy individuals (control group), patients with valvular aortic stenosis (VAS), and patients with aortic incompetence (AI) (Fig. 3f). The average SVA in the control group is 60.93%, whereas that in the VAS and AI groups is 52.13% and 49.06%, respectively; hence, SVA is significantly lower ($p = 6.04 \times 10^{-12}$) in the patients with aorta and aortic valve damage than it is in the control group.

Finally, we demonstrate how SVA can be used to estimate BP continuously. Again, we tested it with the open MIMIC-I dataset. To enable BP tracking, for each subject, we used the 5 sets of measured SVA and reference BPs (with the reference BP's dynamic range encompassing around 70% of the total BP variation for the subject) to calibrate the coefficients in Eq. (4). The total mean absolute errors (MAEs) between the estimated and ground truth SBP and DBP are $\text{MAE}_{\text{SBP}} = 7.92$ mmHg and $\text{MAE}_{\text{DBP}} = 3.77$ mmHg, indicating that the model's estimation accuracy is approaching the IEEE standard of 7 mmHg[27]. (Supplementary Fig. 2). Rapid hemodynamic fluctuations induced by external interventions during ICU operations[28], as well as natural changes in ultradian (12-, 8-, and 6-h) factors[29,30] such as the sympathetic nervous system activity, salt and volume balance, and activation of the renin-angiotensin system, can both lead to the relatively larger errors in this long-term BP dataset. To further improve the measurement accuracy in such scenarios, it may be necessary to include related physiological parameters in the BP estimation model. Figure 3g shows a specific example (patient ID 211 in the MIMIC-I data set, who had a mean SBP and DBP of 170/59 mmHg) of long-term ( > 20 h) continuous BP tracking with the SVA method (based on Eq. (4)). Here we select a challenging case where the hypertensive patient experienced an extremely large BP fluctuation ($\max(SBP)$-$\min(SBP) \approx 150$ mmHg) during the measurement. The SVA-BP model achieved $\text{MAE}_{\text{SBP}}$ of 9.99 mmHg, which is only 6.66% of the ground truth BP dynamic range and 33% of the ground truth SBP standard derivation (30.68 mmHg). The $\text{MAE}_{\text{DBP}}$ is as low as 4.26 mmHg due to the relatively small fluctuation of DBP. The comparison between the ground truth BP and estimated BP distributions (Fig. 3h) validates the capability of the SVA method in tracking BP fluctuation over a large dynamic change. Finally, the variations of SVA and $T_s/T_c$ over time are shown in the lower panel of Fig. 3g, which displays highly consistent patterns ($r = -0.9714$, $p < 0.001$) and demonstrates the long-term reliability of the method for BP tracking.

### Extraction of dynamic SVA using wearable sensor signals

In the previous sections we used the SVA values calculated from BP waveforms, in the following we will demonstrate SVA extraction using wearable sensor signals. The implementation of the SVA method in a wearable device is shown in Fig. 2c. Initially, the user measures his/her cardiac signals (e.g., ECG, PPG, or epidermal pulse) with a wearable or flexible device, thus enabling extraction of the systolic ejection time $T_s$ and cardiac duration $T_c$. The ratio of $T_s$ to $T_c$ and a snapshot BP will be used to infer SVA in Eq. (3).

To validate the aforementioned protocol, we simultaneously measured the BP waveform (which will be used to provide the reference SVA) and ECG, PPG, and epidermal pulse signals of a human subject. During the measurement, the subject was asked to take several deep breaths at random time points, with each deep breath lasting no less than 8 s, to induce signal

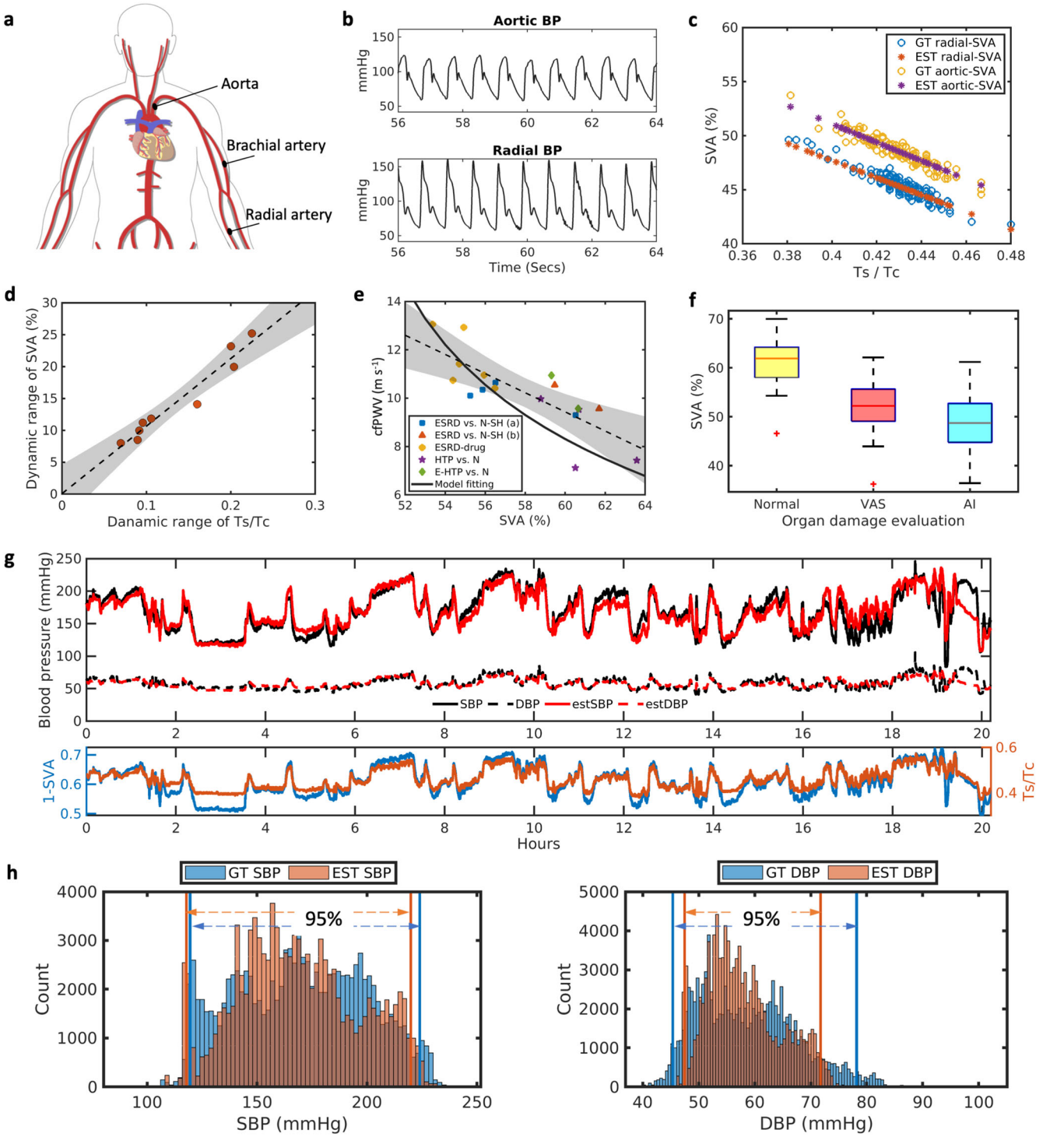


**Fig. 3 | Validation of the SVA method on clinical data sets. a** Illustration of the arterial tree in a human body. From central to peripheral sites: aorta, brachial artery, and radial artery. **b** Typical clinical recordings of aortic and brachial BP waveforms. **c** Inverse relationship between $T_s/T_c$ and the measured/estimated aortic or brachial SVA (%). **d** Relation between the ranges of SVA and $T_s/T_c$. The shaded areas correspond to the 95% CIs of the scope of SVA with $T_s/T_c$. **e** Significant inverse relationship between SVA and cfPWV implying that SVA can be used as an alternative for AS assessment ($p = 9.63 \times 10^{-5}$). The shaded areas correspond to the 95% CIs of the scope of cfPWV with SVA. **f** Differences in the SVA of the normal, VAS, and AI groups, indicating that SVA can be applied for CHD assessment ($p = 6.04 \times 10^{-12}$). **g** Long-term dynamic BP tracking (>20 h) based on the SVA-BP model. **h** Data distributions of the ground truth BP (GT BP) and estimated BP (EST BP) by the SVA-BP model. The 95% intervals of the data distributions are provided for reference.

variations associated with daily activity-triggered hemodynamic changes. To enable SVA calculation in Eq. (3) with ECG, PPG, and epidermal pulse signals, we added a snapshot BP set (i.e., SBP and DBP values) extracted from the BP waveform. The temporally aligned signals for the systolic duration and extracted cardiac cycles are shown in Fig. 4a. The ST interval in the ECG signal [corresponding to left ventricle (LV) contractility] represents the systolic time interval $T_s$, whereas the ECG RR interval is the heartbeat cycle $T_c$[31,32]. Regarding the waveform-based PPG and epidermal pulse signals, the foot-to-dicrotic notch (DN) interval represents $T_s$, and the foot-to-foot interval represents $T_c$[10,32]. We use second-order derivative of the pulse

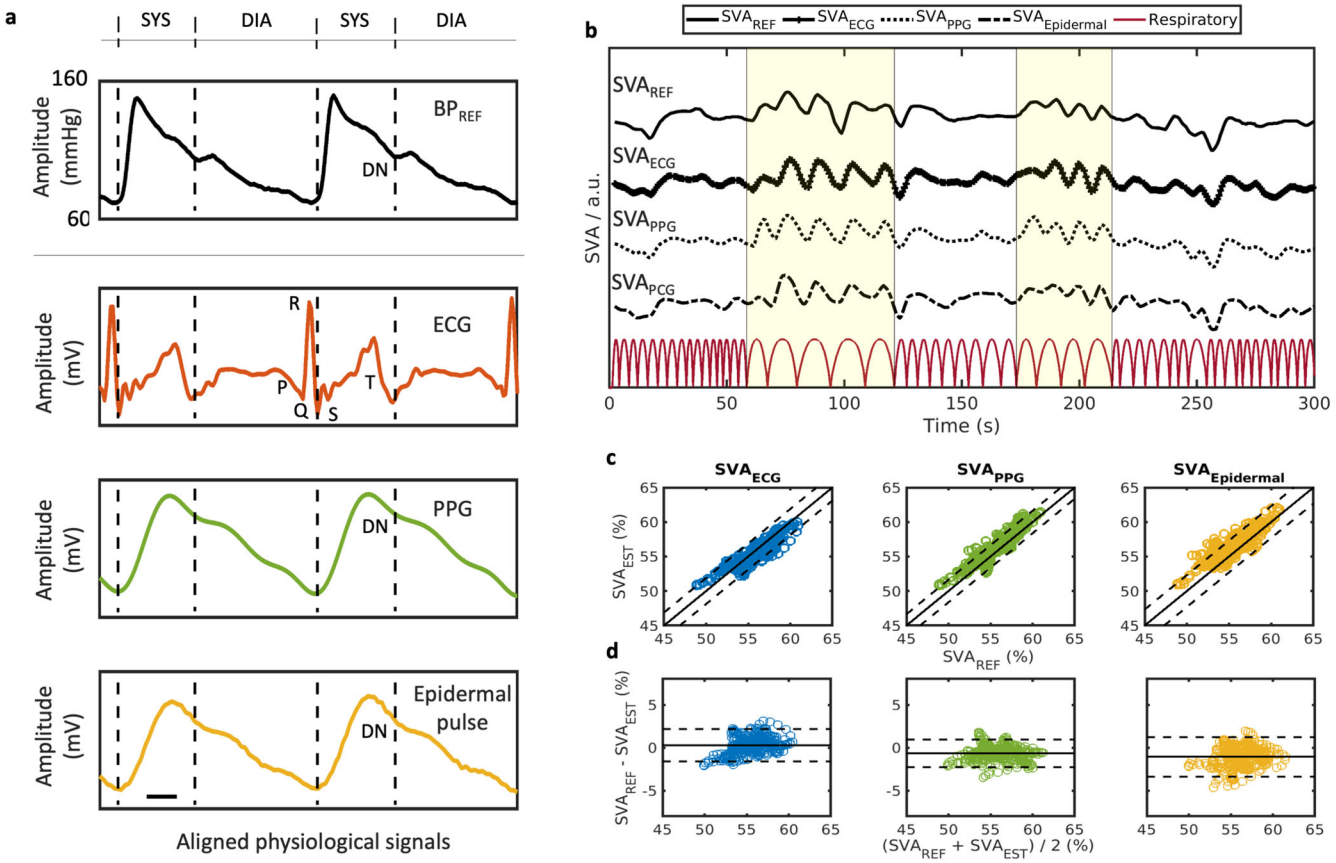


**Fig. 4 | SVA measured by wearable and flexible sensors. a** Reference BP waveform and ECG, PPG, and flexible epidermal pressure signals measured by a Biopac system (BIOPAC Systems Inc., California, USA) from the same subject. Scale bar 100 ms. **b** SVA trends extracted by the sensors during deep breath-induced SVA fluctuations. The reference SVA is extracted from the BP waveform according to Eq. (2). The yellow region indicates deep breathing. **c, d** Correlation and Bland–Altman plots of SVA estimation accuracy for different sensors.

waveform to determine DN point[33]. As shown in Fig. 4b, consistent fluctuations are observed in the SVA acquired from standard BP waveform and various wearable and flexible sensor signals for 383 heartbeat cycles. A comparison of the estimated error and correlation coefficient for the extracted SVA are shown in Fig. 4c, d. The results show that all the estimated SVAs are comparable and that the MAEs are smaller than 1.3%. It is worth noting that despite the PPG and epidermal pulse signals being collected from peripheral sites, which display waveforms differing from the central arterial waveform, they can still be utilized for SVA calculation. This is due to the near-identical time features $T_s$ and $T_c$ observed in both the central BP waveform and peripheral pulse waveforms[34].

### Clinical applications of SVA model-integrated wearable devices

Based on the aforementioned findings, we test the clinical applications of the SVA method with two wearable products, Apple Watch (Apple Inc., California, USA) for providing ECG and INTS finger ring prototype (Intelligent sensing Inc., Hong Kong SAR, China) for providing PPG signals, as shown in Fig. 5a. In the first part of the clinical study, 48 subjects were recruited in Prince of Wales Hospital, Hong Kong, for comparing the vascular aging assessment by SVA and cfPWV. Both INTS-PPG and Apple Watch-ECG are worn by the subjects for acquiring the PPG and ECG signals, and the corresponding snapshot BP and gold standard cfPWV were measured by a commercial Vicorder system simultaneously. Here the SVA was directly calculated using the $T_s/T_c$ values acquired from the wearable device and a snapshot MBP/DBP value. A close relation between age and ECG/PPG-based SVA, identified among subjects of various ages, is observed (upper panel of Fig. 5b). The consistent trends in the increase of (1 – SVA) and cfPWV with the increasing age agree with the theoretical expectation that the proportion of elastic fibers decreases as the arterial wall ages, leading to a decrease in SVA and an increase in cfPWV. Moreover, the lower panel of Fig. 5b reveals that SVA is better correlated with the age groups than is cfPWV, especially for the old-middle and old-young age groups, suggesting that SVA could be a more accurate metric for determining vascular age in middle-aged and elderly patients. Furthermore, we compared the cfPWV and SVA of patients with 34 myocardial infarction who had undergone percutaneous coronary intervention (PCI) and 14 normal individuals (Fig. 5c). The significantly lower SVA of the patients with myocardial infarction who had undergone PCI is consistent with their higher cfPWV, again demonstrating that the SVA method may enable very convenient but clinically valuable AS assessment with wearable consumer electronics.

In the second part of the clinical study, we validated the SVA measurement with the INTS finger ring-acquired PPG and tested its BP tracking performances on 13 subjects. By combining $\delta$ and reference BP measurements in Eqs. (3,4), the coefficients for mapping SVA into BP can be derived, thus enabling BP tracking. The reference continuous BP was collected using a Finometer device (Finapres Medical System, Enschede, Netherlands), and the PPG signal was synchronically recorded with the reference BP. The dynamic SVA was extracted from the PPG signal using the dicrotic notch point-to-foot and foot-to-foot intervals as illustrated in Fig. 4, and the BP was then calculated by feeding the SVA and initial BP values. For each subject, we used the 5 sets of measured SVA and reference BPs (with the reference BP's dynamic range encompassing around 70% of the total BP variation for the subject) to calibrate the coefficients in Eq. (4). Figure 5d and e compares the BP estimation result with the reference, showing excellent agreement with low MAE values of 3.71 and 2.03 mmHg for SBP and DBP respectively (Fig. 5e). These results, together with the long-term BP

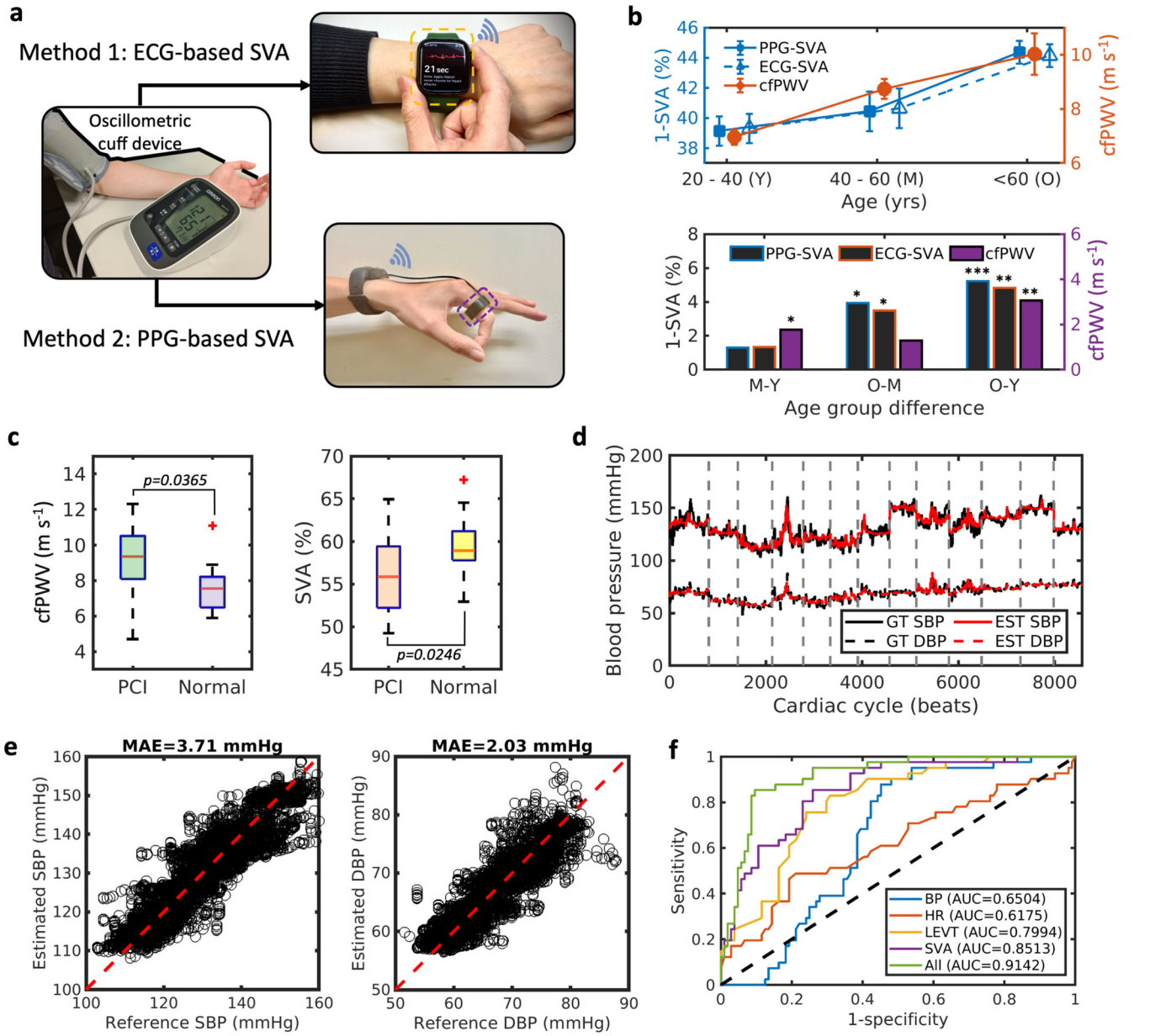


**Fig. 5 | Clinical trials of SVA measurement using commercial wearable devices.** **a** SVA evaluation through the ECG measurements performed with an Apple Watch and PPG measurements performed with an INTS finger ring. **b** Correlations of vascular ageing with SVA and cfPWV. Error bars denote s.d. from the mean. **c** cfPWV and SVA for patients with MI and normal individuals (no. 34/14). **d, e** Dynamic BP tracking performance and statistical BP estimation accuracy of the SVA measurement performed with the PPG-based INTS finger ring. **f** AUCs of various methods for distinguishing normal from poor arterial systems (i.e., patients without and with CHD, no. 41/104).

estimation with the MIMIC-I dataset, demonstrate that the SVA method may enable BP tracking with a single sensing device.

Finally, we classified normal and poor cushioning function in the control group and patient groups (i.e., valvular aortic stenosis[35], aortic incompetence[36], and myocardial infarction) through logistic regression involving SVA and various vital signs. The survey studies are listed in the Supplementary Table 1 under IDs 3 and 5–7. As shown in Fig. 5f, the larger area under the receiver operating characteristic (ROC) curve (Area under the curve (AUC): 0.8513) for SVA indicates that SVA is a better classifier than is BP, *Ts* (i.e., left ventricular ejection time LVET), or *Tc* (i.e., HR). In particular, we note that BP is a limited but relevant indicator for predicting CHD; its AUC is only 0.6504. Combining BP, LVET, HR, and SVA in the logistic regression to produce an all-feature model leads to an AUC of 0.9118. These results confirm that SVA-based wearable devices may be effective for clinical CHD assessment.

## Discussion

In this work, we developed an SVA model that exploits the cushioning function of arteries to identify and track variations in arterial volume. The SVA method can add clinically accurate vascular ageing and CVD assessment functions (i.e., measurements of dynamic arterial stiffness, daily BP fluctuation and CHD severity) to existing wearable/flexible electronics without requiring any modifications to the hardware. In particular, when used with different sensing techniques (e.g., ECG, PPG, and flexible epidermal pulse sensors, etc.), the SVA model was capable of providing consistent and reliable measurement results. Hence, the method can be implemented to nearly all wearable and flexible sensors that can measure heart rhythms; some commercially available examples include the Apple watch[4], Oura-rings[7], Sensora digital stethoscope[37], Withings body cardio scale[38] and smart ears[39]. Although some of these devices require continuous body touch for physiological measurements, e.g., the ECG measurements by

Apple Watch, they can still be used frequently enough to perform CVD evaluation through the SVA model. This means that the technology could be widely deployed at very low cost and with a short launch time.

The results in this study may have important implications for clinical methods in evaluating the development of CVD and CHD. For instance, our experiments show that the SVA (extracted from Apple Watch ECG signals) is better correlated with the age groups than is cfPWV, especially for the old-middle and old-young age groups, suggesting that SVA could be a more accurate metric for determining vascular age in middle-aged and elderly patients. Combing the SVA with a snapshot BP measurement, we achieved continuous BP monitoring at an error level well below the IEEE standard. As the parameters in the SVA-BP model are determined through initial calibration measurements on each subject, it may need to be recalibrated if some hemodynamic changes occur. We note that the SVA model does not include the parameters related to complex neural and humoral regulation of hemodynamic changes over longer time spans, this may lead to deterioration of the performance of the SVA method for BP estimation in some circumstance. Nevertheless, since the core parameters, such as *PSR*, $b$, $b_s^*$, and $k_s^*$, associated with BP estimation (Supplementary note 9) are typically stable for at least a day, we expect the method can support applications such as 24-h ambulatory BP tracking, especially the nocturnal non-dipping BP monitoring. The SVA performance on the MIMIC-I dataset also supports this speculation. Finally, we found that SVA outperforms the commonly used cardiovascular parameters (e.g., BP, heart rate and LVET) in distinguishing CHD. In summary, the SVA model expands the functions of current wearable devices to perform passive, unobtrusive, and clinically meaningful assessment of cardiovascular systems, thus providing a cost-effective telemedicine measurement unit to enable accurate and timely diagnosis and intervention.

## Methods

### Arterial cushioning function described by SVA model

In the systole phase of the cardiac cycle ($0 < t < T_s$), blood is pumped from the left ventricle into the aorta. Some blood is stored in the aorta if the vessel has sufficient compliance, and the remainder is pushed through the action of peripheral vascular resistance (mainly capillaries). The initial pressure is the DBP and $Q_{in}$ is the input blood flow. The physical process can be described mathematically as follows:

$$\begin{cases} C\frac{dP(t)}{dt} + \frac{P(t)}{R} = I(t) \\ P(0) = DBP\,(as\ t = 0) \\ I(t) = Q_{in} \end{cases} \quad (5)$$

In the diastolic phase ($T_s < t_T$), the aortic valve is closed; hence, no blood is pumped to the peripheral vascular artery. Volume stored in the elastic aorta (compliance) is transferred to the peripheral artery and organ during the diastolic period. The initial pressure corresponds to the pressure once the aortic valve has closed. The diastolic phase can be described as follows:

$$\begin{cases} C\frac{dP(t)}{dt} + \frac{P(t)}{R} = I(t) \\ P(T_s) = P_s^{dn}(as\ t = T_s) \\ I(t) = 0 \end{cases} \quad (6)$$

where $C$ is arterial compliance, $R$ is the systematic vascular resistance, $I(t)$ is the aortic blood flow, $P$ is the aortic pressure, and $P_s^{dn}$ is dicrotic notch pressure. By solving Eqs. (5) and (6) under the constraint that the aortic compliance is SV/PP[23], SVA can be obtained (details in Supplementary Note 2).

### Invasive aorta and radial pressure measurements for SVA validation

The central pressure in the aorta and the radial BP were measured from a patient with CVD through invasive Millar pressure monitoring at a sampling rate of 1000 Hz. The clinical trial was conducted in Prince of Wales Hospital, Hong Kong. The experiment was approved by the Joint Chinese University of Hong Kong–New Territories East Cluster Clinical Research Ethics Committee and received consent from the patient. For cross-validation we also tested our model on the radial BP data from the open MIMIC-I database provided by Boston's Beth Israel Hospital, United States[28,40], which includes real-time clinical recordings from the ICU patients. This database provides long data recordings (average duration > 20 h), which are suitable for validating SVA and BP tracking. All collected signals had a sampling rate of 125 Hz. In this study, we focused on patients with an obvious DN of the arterial BP to extract $T_s$ and $T_c$ for validating the SVA model. Hence, the nine data recordings were analyzed. The measured parameters are summarized in the Supplementary Table 1 under IDs 2 and 5.

### Clinical measurement of SVA and its relation with AS and organ damage

We conducted clinical studies on open data sets to explore the relationship between cfPWV and SVA for patients from different studies and populations, such as healthy individuals, patients with end-stage renal disease[41–43], normotensive men and women[44], and subjects with hypertension[45]; the results are summarized in the Supplementary Table 1 under IDs 9–13. In addition, we explored using SVA to evaluate heart damage in valvular aortic stenosis[35], aortic incompetence[36], and normal groups[46] by using data from open data sets. The data are summarized in the Supplementary Table 1 under IDs 6–8. The data sets contained the key cardiovascular parameters—BP, $T_s$ (i.e., LVET), and $T_c$ (i.e., heartbeat period)—for each patient; hence, individual-specific SVAs could be calculated using Eq. (3).

### SVA estimation-based wearable and flexible sensor signals

ECG, PPG, flexible epidermal pulse, and BP measurements were collected to compare the accuracy of each technique for SVA estimation. In this experiment, one participant was recruited. During data collection, the participant was asked to relax and sit in a chair. The Biopac MP150 system (BIOPAC system inc. California, USA) with ECG100C, PPG100C, RSP100C, and Cnap-NIBP 100D with BP waveform measurement was employed. On the other hand, a flexible epidermal pulse sensor developed from our previous study was carried out to measure the pressure pulse[5]. The signals are recorded and synchronized based on the specific time slots that mark the start and end of data recording. Hence, this allows us to make ECG, PPG, and flexible epidermal pulse recordings and to measure the respiratory rate and BP simultaneously in two physiological states (rest and deep breathing). Data were collected for about 5 min at a sampling rate of 1000 Hz for Biopac system and of about 50 Hz for the epidermal pulse recording system (through a high-speed Keithley sourcemeter - Model 2612 A, up to 50 KHz sampling rate[5]). This data set was constructed mainly to determine whether the SVA method could track abrupt respiratory changes. All extracted parameters are summarized in the Supplementary Table 1 under ID 1.

### Clinical trials on vascular age and CVD assessment using commercial wearable devices

We recruited 48 subjects (34 patients with myocardial infarction and 14 healthy individuals as control subjects) covering the age range of 20–90 years at the Prince of Wales Hospital in Hong Kong to conduct vascular ageing, AS and organ damage studies with a wearable device (Joint CUHK-NTEC CREC Ref. No.: 2022.335). We used commercially available wearable products (i.e., Apple Watch and INTS finger ring) to extract each participant's cardiac rhythm and thus measure their SVA. To be specific, before the measurement, the participant was asked to rest and lie on a bed. The Vicorder system was used to perform gold standard cfPWV measurements for AS assessment. Two deflatable cuffs were carefully attached to their carotid and femoral artery sites, and the operator checked the position of the cuffs and measured the distance between the aforementioned sites. After all required patient information had been collected and entered into the

Vicorder system, the system began recording carotid and femoral pulses simultaneously. The system calculated the ratio of the distance between the carotid and femoral pulses and their foot-to-foot time interval and output the cfPWV at a sampling rate of 556 Hz. Besides, for comparison, A 30-second ECG signal was recorded with 512 Hz sampling rate by holding a finger from the nonwatch hand on the Apple watch. Meanwhile, the INTS finger ring with 250 Hz sampling rate was attached to the subject's index finger to acquire the PPG signal within 1 min. Cuff-based BP was simultaneously measured using the Vicorder system. In view of the fact that signal acquisition can be accomplished within a time span of under 1 minute, it guarantees the uniformity of physiological parameters by both wearable devices. All extracted parameters are summarized in the Supplementary Table 1 under ID 3.

Furthermore, we also demonstrated the INTS PPG-based wearable finger ring can be used on daily BP tracking. The PPG ring has a wired connection between the PPG module with a photodetector and a digital processing chip. Real-time PPG data are compressed, transmitted over Bluetooth, and eventually stored in the cloud. In our protocol, the PPG signal was collected in reflection mode while the PPG ring was attached to the subject's index finger. We recruited 13 participants aged >65 years. At the beginning of the measurement, the participant was asked to remain calm and relax their left arm and fingers for 2 minutes. The PPG and reference BP (obtained using a noninvasive continuous BP measurement Finapres system) were recorded for approximately 10 minutes. The Finapres BP measurement signals and ring PPG signals could be set to record at the same heartbeat cycle, ensuring that the devices were synchronized. The foot-to-DN and foot-to-foot intervals of the ring PPG signal were used to calculate SVA. All extracted parameters in this dataset are summarized in the Supplementary Table 1 under ID 4.

### Statistical analysis

Signal parameters were extracted and calculated using MATLAB R2022a. Various statistical analysis metrics were calculated, including ROC, AUC, sensitivity, specificity, and 95% CI, and correlation plots were produced using MATLAB. Simple correlation analysis was performed using the Pearson correlation method, and methodological consistency was tested using the two-sample *t*-test. A linear regression equation for SVA and cfPWV was obtained and used to analyze the consistency of the estimated and reference SVA. Statistical significance was indicated by $p < 0.05$ (*), $< 0.01$ (**), and $< 0.001$ (***). The MAE was used to evaluate the accuracy of SVA for BP estimation.

## Data availability

Data generated in this study are provided in the Main Text and the Supplementary Information. Additional data are available from the corresponding author upon request.

## Code availability

All codes that support the findings of this study are available from the corresponding authors upon reasonable request.

Received: 3 October 2023; Accepted: 15 March 2024;
Published online: 16 April 2024

## References

1. WHO. Ageing and health. https://www.who.int/news-room/fact-sheets/detail/ageing-and-health (2022).
2. Olsen, M. H. et al. A call to action and a lifecourse strategy to address the global burden of raised blood pressure on current and future generations: the Lancet Commission on hypertension. *Lancet* **388**, 2665–2712 (2016).
3. Lozano, R. et al. Global and regional mortality from 235 causes of death for 20 age groups in 1990 and 2010: a systematic analysis for the Global Burden of Disease Study 2010. *Lancet* **380**, 2095–2128 (2012).
4. Marcus, G. M. The Apple Watch can detect atrial fibrillation: so what now? *Nat. Rev. Cardiol.* **17**, 135–136 (2020).
5. Luo, N. et al. Hollow-structured graphene-silicone-composite-based piezoresistive sensors: Decoupled property tuning and bending reliability. *Adv. Mater.* **29**, 1702675 (2017).
6. Elgendi, M. et al. The use of photoplethysmography for assessing hypertension. *NPJ Digit. Med.* **2**, 60 (2019).
7. Pho, G. N., Thigpen, N., Patel, S. & Tily, H. Feasibility of Measuring Physiological Responses to Breakthrough Infections and COVID-19 Vaccine Using a Wearable Ring Sensor. *Digit. Biomark.* **7**, 1–6 (2023).
8. Ford, T. J. et al. Assessment of vascular dysfunction in patients without obstructive coronary artery disease: why, how, and when. *Cardiovasc. Interv.* **13**, 1847–1864 (2020).
9. Chirinos, J. A., Segers, P., Hughes, T. & Townsend, R. Large-Artery Stiffness in Health and Disease: JACC State-of-the-Art Review. *J. Am. Coll. Cardiol.* **74**, 1237–1263 (2019).
10. Vlachopoulos C., O'Rourke M., and Nichols W. W., *McDonald's Blood Flow in Arteries: Theoretical, Experimental and Clinical Principles* Ch. 20 (CRC Press, 2011).
11. Laurent, S. & Boutouyrie, P. Arterial Stiffness and Hypertension in the Elderly. *Front. Cardiovasc. Med.* **7**, 544302 (2020).
12. Reference Values for Arterial Stiffness, C. Determinants of pulse wave velocity in healthy people and in the presence of cardiovascular risk factors: 'establishing normal and reference values'. *Eur. Heart J.* **31**, 2338–2350 (2010).
13. Solà J., Delgado R. *The Handbook of Cuffless Blood Pressure Monitoring: A Practical Guide for Clinicians, Researchers, and Engineers* Ch. 6 (Cham: Springer, 2019).
14. Pandit, J. A., Lores, E. & Batlle, D. Cuffless Blood Pressure Monitoring: Promises and Challenges. *Clin. J. Am. Soc. Nephrol.* **15**, 1531–1538 (2020).
15. Westerhof N., Stergiopulos N., Noble M. I. M., Westerhof B. E. *Snapshots of hemodynamics: an aid for clinical research and graduate education* Ch. 10 (New York: Springer, 2019).
16. Bank, A. J. et al. Contribution of collagen, elastin, and smooth muscle to in vivo human brachial artery wall stress and elastic modulus. *Circulation* **94**, 3263–3270 (1996).
17. Dobrin, P. B. Mechanical Properties of Arteries. *Physiol. Rev.* **58**, 397–460 (1978).
18. Greenwald, S. E. Ageing of the conduit arteries. *J. Pathol.* **211**, 157–172 (2007).
19. Stefanadis, C. et al. Aortic stiffness as a risk factor for recurrent acute coronary events in patients with ischaemic heart disease. *Eur. Heart J.* **21**(5), 390–396 (2000).
20. Hachicha, Z., Dumesnil, J. G., Bogaty, P. & Pibarot, P. Paradoxical low-flow, low-gradient severe aortic stenosis despite preserved ejection fraction is associated with higher afterload and reduced survival. *Circulation* **115**, 2856–2864 (2007).
21. Westerhof, N., Lankhaar, J. W. & Westerhof, B. E. The arterial Windkessel. *Med Biol. Eng. Comput* **47**, 131–141 (2009).
22. Belz, G. G. Elastic properties and Windkessel function of the human aorta. *Cardiovasc. Drugs Ther.* **9**, 73–83 (1995).
23. Kuecherer, H. F., Just, A. & Kirchheim, H. Evaluation of aortic compliance in humans. *Am. J. Physiol. Heart Circ.* **278**, H1411–H1413 (2000).
24. Fortier, C. & Agharazii, M. Arterial Stiffness Gradient. *Pulse (Basel)* **3**, 159–166 (2016).
25. Gavish, B. & Izzo, J. L. Jr Arterial Stiffness: Going a Step Beyond. *Am. J. Hypertens.* **29**, 1223–1233 (2016).
26. Tomitani, N., Kanegae, H. & Kario, K. The effect of psychological stress and physical activity on ambulatory blood pressure variability detected by a multisensor ambulatory blood pressure monitoring device. *Hypertens. Res.* **46**, 916–921 (2023).
27. IEEE Standard for Wearable, Cuffless Blood Pressure Measuring Devices. *IEEE Standard 1708-2014*. (2014).

28. Moody, G. B., Mark., R. G. A database to support development and evaluation of intelligent intensive care monitoring. *Comput. In Cardiol*., 657-660 (1996).
29. Perez-Lloret, S., Aguirre, A. G., Cardinali, D. P. & Toblli, J. E. Disruption of ultradian and circadian rhythms of blood pressure in nondipper hypertensive patients. *Hypertension* **44**, 311–315 (2004).
30. Peixoto, A. J. & White, W. B. Circadian blood pressure: clinical implications based on the pathophysiology of its variability. *Kidney Int* **71**, 855–860 (2007).
31. Alhakak, A. S. et al. The significance of left ventricular ejection time in heart failure with reduced ejection fraction. *Eur. J. Heart Fail.* **23**, 541–551 (2021).
32. Berne, L. *Physiology* Ch. 16 (Elsevier Health Sciences, 2018).
33. Oppenheim, M. I. & Sittig, D. F. An innovative dicrotic notch detection algorithm which combines rule-based logic with digital signal processing techniques. *Comput. Biomed. Res.* **28**, 154–170 (1995).
34. Adji, A., Hirata, K. & O'Rourke, M. F. Clinical use of indices determined non-invasively from the radial and carotid pressure waveforms. *Blood Press. Monit.* **11**, 215–221 (2006).
35. Bache, R. J., Wang, Y. & Greenfield, J. C. Jr Left ventricular ejection time in valvular aortic stenosis. *Circulation* **47**, 527–533 (1973).
36. Luomanmaki, K. & Heikkila, J. Estimation of the severity of aortic incompetence from prolongation of the left ventricular ejection time. *Acta Med. Scand.* **1-2**, 107–114 (1970).
37. Sensora, E. Structural murmur detection. https://www.ekohealth.com/blogs/newsroom/eko-biospace-07122022 (2022).
38. Collier, S. R. et al. Withings Body Cardio versus Gold Standards of Pulse-Wave Velocity and Body Composition. *J. Pers. Med.* **10**, 17 (2020).
39. Ltd., W.B.D. WBD101. https://www.wbd101.net/activhearts (2023)
40. Goldberger, A. L. et al. PhysioBank, PhysioToolkit, and PhysioNet. *Circulation* **101**, e215–e220 (2000).
41. London, G. et al. Increased systolic pressure in chronic uremia. Role of arterial wave reflections. *Hypertension* **20**, 10–19 (1992).
42. London, G. M. et al. Cardiac hypertrophy, aortic compliance, peripheral resistance, and wave reflection in end-stage renal disease. Comparative effects of ACE inhibition and calcium channel blockade. *Circulation* **90**, 2786–2796 (1994).
43. London, G. M. et al. Cardiac and arterial interactions in end-stage renal disease. *Kidney Int* **50**, 600–608 (1996).
44. GM, L. Influence of sex on arterial hemodynamics and blood pressure. *Hypertension* **26**, 514–519 (1995).
45. London, G. M., Pannier, B. & Safar, M. E. Arterial Stiffness Gradient, Systemic Reflection Coefficient, and Pulsatile Pressure Wave Transmission in Essential Hypertension. *Hypertension* **74**, 1366–1372 (2019).
46. Hasegawa, M., Rodbard, D. & Kinoshita, Y. Timing of the Carotid Arterial Sounds in Normal Adult Men: Measurement of Left Ventricular Ejection, Pre-Ejection Period and Pulse Transmission Time. *Cardiology* **78**, 138–149 (1991).


## Acknowledgements

This work was supported in part by the Excellent Young Scientists Fund from National Natural Science Foundation of China under Grant 62022004, in part by the Shenzhen-Hong Kong-Macau Technology Research Programme (Type C) from Science, Technology and Innovation Commission of Shenzhen Municipality (STIC) under the Grant SGDX20220530111200001 and in part by the Hong Kong Centre for Cerebro-cardiovascular Health Engineering under the InnoHK Scheme of Hong Kong SAR. The authors would like to thank Sze-Kei Lau, Shirley Li, Ken Wong, Shun Wu, and Lei Zhao for their assistance in the clinical experiment at Prince Wales Hospital. We also thank Yihao Li and Zhou Jiang for their assistance in conducting the flexible sensor measurements, and all the volunteers for their cooperation in the experiments.

## Author contributions

The work was conceptualized by S.Q. and N.Z. The models were derived by S.Q., and experiments were designed by S.Q., N.Z. and B.Y. Wearable and flexible devices were investigated by N.Z. and B.Y. Data analysis and result visualization were conducted by S.Q. and N.Z. Funding acquisition and project administration were provided by N.Z. The original manuscript was written by S.Q., N.Z. and B.Y. All authors participated in scientific planning, discussions of the results, and final approval of the completed version.

## Competing interests

The authors declare no competing interests.

## Additional information

**Supplementary information** The online version contains supplementary material available at https://doi.org/10.1038/s41528-024-00307-1.

**Correspondence** and requests for materials should be addressed to Ni Zhao.